TURBULENCE STRUCTURE OVER ALIGNED AND INCLINED RIBS IN ADVERSE PRESSURE GRADIENT

Jonathan M. Tsikata and Mark F. Tachie
Department of Mechanical and Manufacturing Engineering
University of Manitoba
E2-327 EITC, 75A Chancellors Circle, Winnipeg, MB. R3T 5V6 Canada
tachiemf@cc.umanitoba.ca

ABSTRACT

This paper reports an experimental study of fully developed channel and adverse pressure gradient (APG) turbulent flows over transverse square ribs inclined at 90° and 45° to the approach flow. A particle image velocimetry (PIV) system was used to conduct velocity measurements in the streamwise-wall-normal plane in order to study the structural features of the flow over these rib configurations as well as the effects of APG on the flow. The results demonstrate that APG enhanced turbulence level compared to the fully developed channel flow. On the other hand, the 45° ribs decreased drag compared to 90° ribs. The two-point velocity correlations revealed that the inclination as well as the size of the hairpin packets varies with rib inclination and pressure gradient.

INTRODUCTION

Turbulent flows over rough walls are encountered in many engineering and industrial applications. Examples include flows over turbine and compressor blades. The roughness directly affects the flow characteristics, at least in the immediate vicinity of the wall. These effects may include enhanced mixing as well as mass, momentum and convective heat transport. In view of their diverse applications, numerous studies have been conducted in the past to understand the effects of wall roughness on both the velocity and thermal fields in wall-bounded flows.

The roughness elements that are used to model surface roughness are generally classified into two-dimensional and three-dimensional roughness elements. Two-dimensional roughness elements such as transverse square ribs are also used in many industrial applications to augment convective heat transfer, for example, in heat exchangers, cooling system of gas turbines and nuclear reactors. In these applications, the ribs are often inclined at an angle to the approach flow. Prior research on the thermal field demonstrated that inclined ribs augment convective heat transfer better than ribs positioned perpendicular to the approach flow (Han et al., 1978). However, there are limited velocity field studies on inclined ribs (Bonhoff et al., 1999; Gao and Sunden, 2004; Tachie and Shah, 2008). These studies revealed that inclined ribs produce lower drag in comparison to perpendicularly positioned ribs. Previous studies (e.g. Nagano and Tagawa, 1995) demonstrated that coherent structures play an essential role in the mechanisms responsible for momentum and convective heat transfer. Therefore, an in-depth understanding of the velocity fields and coherent structures in turbulent flows over inclined ribs will lead to an efficient design of fluid engineering devices such as heat exchangers and gas turbines.

The flow fields over rough walls may also be affected by a mean pressure gradient. For example, an adverse pressure gradient is encountered in turbines and diffusers. In contrast to zero pressure gradient and fully developed channel flows, APG turbulent flows over rough walls have not been studied in detail. The few studies on the combined effects of roughness and APG on the turbulence characteristics include the pitot tube experiments by Perry et al. (1969), and PIV measurements by Tachie (2007) and Tay et al. (2009).

The objective of this paper is to study the effects of APG and rib inclination on the mean flow and turbulence statistics. A PIV system is used to conduct detail velocity measurements over ribs in a channel that consists of an upstream parallel section to produce a fully developed channel flow and a diverging section to produce an APG flow. The ribs were attached to the lower straight wall of the channel at inclination angles of 90° and 45° to the approach flow.

EXPERIMENTAL SET-UP

The test channel was fabricated from 6 mm thick clear acrylic plates and was inserted into the test section of an existing water tunnel which is 2.5 m long, 0.2 m wide and 0.2 m deep. Figure 1 shows the side view of the test channel as well as a typical rib configuration. As shown in the figure, the first 1500 mm of the channel (*OA*) and the last 400 mm of the channel (*BC*) have straight parallel upper and lower walls. The upper wall of the 600 mm section of the channel (*AB*) located between these parallel sections diverges linearly from a height of $2h$ = 55.5 mm to 96.5 mm at an inclination angle of 4°. The internal width of the channel was $2B$ = 186 mm. Therefore, the aspect ratio of the channel varies from 3.35 at the inlet parallel section to 1.93 at the end of the diverging section. As shown in Figure 1, the streamwise, wall-normal and spanwise directions are along the x, y and z axes, respectively; $x = 0$ is at the inlet to the 55.5 mm × 186 mm section, $y = 0$ at the top plane of the ribs, and $z = 0$ at the mid-span of the channel.

Two-dimensional transverse square ribs with nominal height of k = 3 mm were used as the roughness elements. The ribs spanned across the entire width of the channel, and they were secured to the straight lower wall of the channel with a

thin double sided tape (Figure 1b). The pitch, p, measured as the perpendicular distance between any two adjacent ribs was maintained at $p = 8k$. The ribs were inclined at $\alpha = 90°$ and 45° to the approach flow (Figure 1b). Following Bonhoff et al. (1999), the edges of the 45° ribs pointing to the upstream and downstream sections of the channel are referred to as the leading and trailing edges, respectively.

The PIV system comprised of an Nd-YAG laser and HiSense 4M camera. The flow was seeded with 10 μm silver coated hollow glass spheres. For each rib configuration, measurements were made in planes located in the upstream parallel section (S_P) and diverging section (S_D). For the 45° ribs, measurements were made in the x-y plane at mid-span (z = 0 mm or P_O), close to the leading edge (z = +45 mm or P_L) and close to the trailing edge (z = −45 mm or P_T). For the 90° ribs, measurements were made in the x-y plane at z = 0 mm only. The notation $\alpha_{90}S_PP_O$ is used to represent test condition for 90° ribs in the parallel section and measurement plane at z = 0 mm. Similarly, $\alpha_{45}S_DP_L$ represents test condition for 45° ribs in the diverging section and measurement plane at z = +45 mm. The field of view was approximately 49 mm × 49 mm in both the parallel and diverging sections. It should be noted that in the diverging section, the lower and the upper boundary layers were measured separately using a similar field of view (Figure 1a). This is necessary to maintain a similar spatial resolution in the upstream parallel and diverging sections. The flow statistics were computed from 6000 instantaneous image pairs using adaptive-correlation at interrogation area of $\Delta x \times \Delta y$ = 32 × 32 pixels with 50% overlap. The profiles reported in the subsequent sections are spatial averaged results obtained over a pitch. The uncertainty in the mean velocity at 95% confidence level was estimated to be ±2% and that for the Reynolds stresses was ±10% close to the ribs. Also, the measurement uncertainty in the estimated C_f is ±10%.

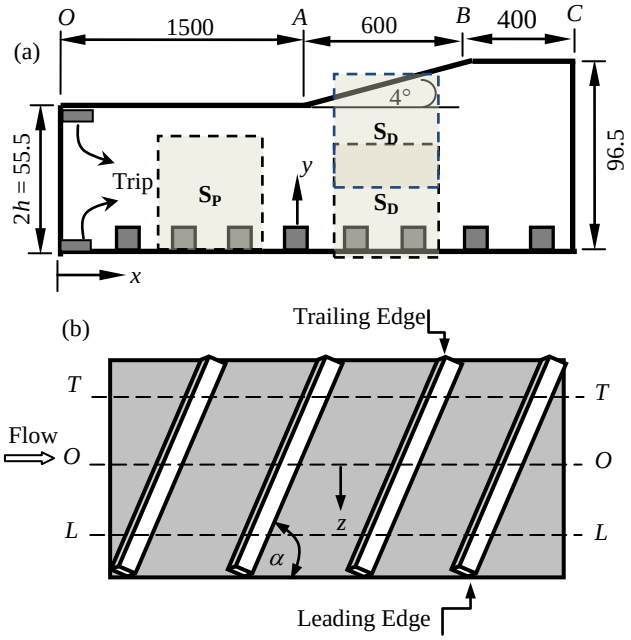

Figure 1. Schematic of test section and rib configurations (not to scale): (a) test section, (b) ribs inclined at α. LL indicates measurement plane close to the leading edge (z = +45 mm), OO at mid-span (i.e. at z = 0 mm) and TT is close to the trailing edge (z = −45 mm). All dimensions in mm.

RESULTS AND DISCUSSION

Effects of Pressure Gradient and Rib Inclination

In this section, the flow characteristics obtained at the mid-span of the channel are used to study the effects of rib inclination and pressure gradient on the flow. The test conditions as well as the boundary layer parameters are reported in Table 1. In this table, U_m is the spatial average maximum streamwise mean velocity, δ is the boundary layer thickness, θ is momentum thickness, H is the shape factor, K (= $(\nu/U_m^2)(dU_m/dx)$) is the dimensionless pressure gradient parameter and Re_θ (= $\theta U_m/\nu$) is the Reynolds number. Table 1 shows that over the 90° ribs, APG reduced U_m by 21% compared to the upstream value. Besides, δ, θ and H in the diverging section are respectively, 50%, 68% and 27% larger than the corresponding upstream values. Similar increase in δ and θ with APG was reported by Tachie (2007). At the mid-span of 45° ribs, APG decreased U_m, δ and θ by 21%, 48% and 38% but the difference in H is only 5%. As expected, K is positive in the upstream parallel section and negative in the diverging section. The table also demonstrates that δ, θ and H are considerable lower over the 45° ribs than over the 90° ribs. These observations are consistent with previous results (Tachie and Shah, 2008).

Figure 2a shows the mean velocity profiles at mid-span together with the DNS data from Ikeda and Durbin (2007). The measured data over the 90° ribs in the parallel section ($\alpha_{90}S_PP_O$) agree reasonably well with the DNS results. In accordance with previous studies, it is observed that the profiles in the diverging section are less uniform than the corresponding profiles in the parallel section. For example, at y/δ = 0.40, U/U_m decreased from 0.70 in the upstream parallel section to 0.56 in the diverging section over the 90° ribs. APG also made the profiles less uniform over the 45° ribs, albeit less dramatic than observed over the 90° ribs. For example, at y/δ = 0.40, U/U_m decreased from 0.86 in the upstream parallel section to 0.82 in the diverging section over the 45° ribs. More importantly, the profiles over the 90° ribs are less uniform than those over 45° ribs, irrespective of the pressure gradient.

Table 1. Summary of boundary layer characteristics.

Test	α °	U_m m/s	δ mm	θ mm	H	K × 10^{-7}	Re_θ
$\alpha_{90}S_PP_O$	90	0.380	38.4	5.6	1.86	1.93	2120
$\alpha_{90}S_DP_O$	90	0.300	57.4	9.4	2.37	−26.59	2820
$\alpha_{45}S_PP_O$	45	0.364	26.8	2.9	1.49	1.51	1040
$\alpha_{45}S_DP_O$	45	0.289	14.0	1.8	1.56	−30.88	510
$\alpha_{45}S_PP_L$	45	0.402	22.1	2.0	1.44	4.45	790
$\alpha_{45}S_DP_L$	45	0.347	10.6	1.3	1.78	−19.53	470
$\alpha_{45}S_PP_T$	45	0.303	16.9	2.0	1.95	1.31	600
$\alpha_{45}S_DP_T$	45	0.257	17.4	2.3	1.79	−36.37	580

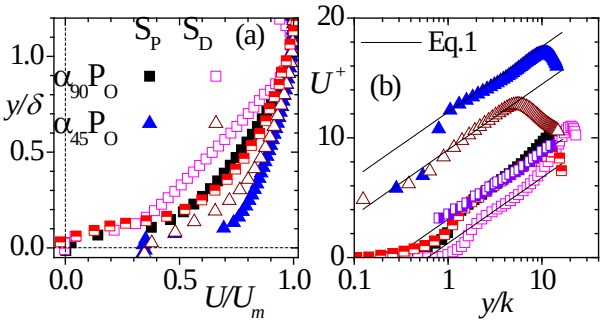

Figure 2. Mean velocity profiles at mid-span of the channel: (a) outer coordinates (b) inner coordinates. Symbols: Hanjalic and Launder (1972): ◨; and Ikeda and Durbin (2007): ⬒.

Figure 2b shows the mean velocity profiles at mid-span of the 45° and 90° ribs in the following log-law format adopted by Hanjalic and Launder (1972):

$$U^+ = 2.38\log(y/k) + C \qquad (1)$$

where C is a constant. The same relation with C = 3.2 was used by Ikeda and Durbin (2007). Figure 2b shows that the profile for $\alpha_{90}S_PP_O$ is in good agreement with the DNS and hot-wire results. For a given rib inclination, APG tends to shift the mean profile downward relative to the profile in the parallel section. Besides, the plots show that, irrespective of pressure gradient, the mean profiles over the 90° ribs are shifted downwards relative to profiles over the 45°. As shown in Table 2, the log-law constant C obtained for $\alpha_{90}S_PP_O$ is similar to the value reported in the previous DNS and hot-wire studies; however, the value of C varies with rib inclination as well as pressure gradient. The mean velocity profiles were also plotted in the classical log-law format (not shown) from which the roughness characteristics were estimated. The summary provided in Table 2 shows that APG decreased the friction coefficient, C_f , over the 90° ribs by 9% but increased C_f by 79% over the 45° ribs. Moreover, C_f over the 45° ribs is decreased by 63% in parallel section and 27% in the diverging section in comparison to the corresponding values obtained over the 90° ribs. Tachie and Shah (2008) also observed a 37% reduction in C_f for 45° ribs compared to 90° ribs in a channel roughened with ribs on both the lower and upper walls. The roughness shift (ΔB, measured relative to classical log-law formulation for a smooth wall), is larger for the 90° ribs than the 45° ribs. Based on the criterion proposed by Schlichting (1979) for k_s^+ (equivalent sand grain roughness parameter), the roughness regime at the mid-span of the 45° rib is in the transitionally rough regime (since $5 < k_s^+ < 70$) whereas that for the 90° rib is in the fully rough regime (since $k_s^+ > 70$). The table also indicates that the diameter of mono disperse equivalent sand grains required to produce the same amount of flow resistance over the ribs increases with APG, and is larger for the 90° rib than for 45° ribs.

Figures 3a-3c show the distribution of the Reynolds stresses. The stresses and the wall-normal distance are normalized, respectively, by U_τ^2 and y_{uv}, where y_{uv} corresponds to the y-location where the Reynolds shear stress ($-uv$) changes sign. The profiles obtained in the parallel section ($\alpha_{90}S_PP_O$) collapsed reasonably well with the

Table 2. Summary of drag characteristics.

Test	U_τ m/s	C_f	C	ΔB	k_s^+	k_s/k
$\alpha_{90}S_PP_O$	0.0363	0.0182	3.20	13.1	914	7.4
$\alpha_{90}S_DP_O$	0.0274	0.0166	1.20	14.8	1799	21.9
$\alpha_{45}S_PP_O$	0.0213	0.0068	12.15	3.0	14	0.2
$\alpha_{45}S_DP_O$	0.0226	0.0122	9.00	6.5	60	0.9
$\alpha_{45}S_PP_L$	0.0268	0.0089	10.50	5.2	36	0.4
$\alpha_{45}S_DP_L$	0.0295	0.0145	8.65	7.2	81	0.9
$\alpha_{45}S_PP_T$	0.0232	0.0117	8.90	6.4	59	0.8
$\alpha_{45}S_DP_T$	0.0209	0.0132	8.0	7.1	78	1.3

data from Hanjalic and Launder (1972) and Ikeda and Durbin (2007) except in the region $y/y_{uv} < 0.50$ where the u^{+2}-profile of Hanjalic and Launder (1972) is typically larger than the present data. In general, Figure 3 demonstrates that over the 90° ribs, the Reynolds stresses are noticeably higher in the diverging section than in the parallel section. The increase in v^{+2} in the diverging section is an indication that there exists a larger angular excursion of the wall-normal instantaneous velocity vectors in the presence of APG. Over the 45° ribs, the distribution of u^{+2} is not significantly affected by APG. Close to the 45° ribs, APG decreased v^{+2} and $-u^+v^+$, but for $y/y_{uv} >$ 0.40 APG augments v^{+2}. For $y/y_{uv} > 0.21$, the distribution of $-u^+v^+$ over the 45° ribs is independent of APG. The plots also show that in the parallel section, the effects of rib inclination on u^{+2} and $-u^+v^+$ is negligible for $y/y_{uv} > 0.12$, but v^{+2} is enhanced over the 45° ribs compared to 90° ribs. These observations are in sharp contrast to that of Tachie and Shah (2008) that 45° ribs reduce turbulence level. In the diverging section, the 90° ribs augment the stresses compared to that over 45° ribs.

The effects of APG and rib inclination on the turbulence motions are also studied using Townsend structure parameter, a_1. Because the spanwise component of the velocity

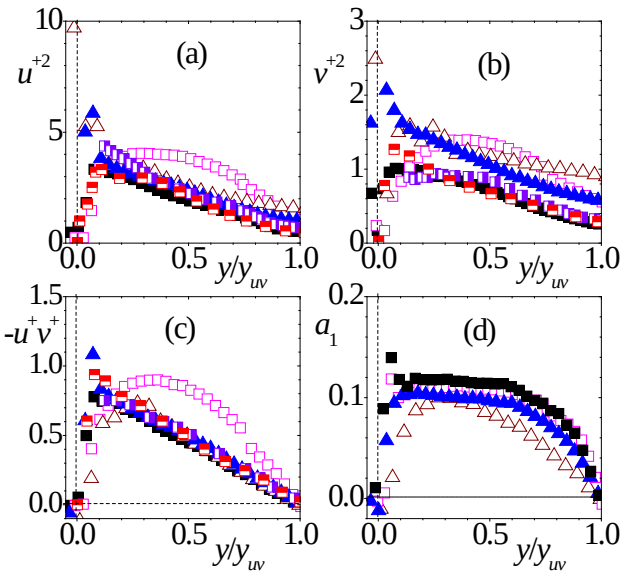

Figure 3. Reynolds stresses and Townsend structure parameter at mid-span of the channel. Symbols as in Figure 2.

fluctuation was not measured in the present study, the following estimate was used: $a_1 = -uv/(1.5(u^2 + v^2))$. Figure 3d demonstrates that a_1 is lower than a typical value of 0.15 reported in a turbulent boundary layer by Bradshaw (1967). The distribution of a_1 is reduced by APG in the diverging section compared to the value obtained in the parallel section. In both the parallel and diverging sections, the distribution of a_1 is higher over 90° ribs than over the 45° ribs. The observed differences in the distribution of a_1 in the parallel and diverging sections suggest that the type of mechanism resulting in the production and redistribution of turbulence is dependent on pressure gradient and rib inclination.

Effects Spanwise Measurement Plane Location

Table 1 demonstrates that in the upstream parallel section of the 45° ribs, the value of U_m close to the leading edge ($\alpha_{45}S_PP_L$) is 10% higher than the value obtained at the mid-span ($\alpha_{45}S_PP_O$), whereas the value close to the trailing edge ($\alpha_{45}S_PP_T$) is 17% lower. Similarly, in the diverging section, U_m is 20% higher close to the leading edge ($\alpha_{45}S_DP_L$) and 11% lower close to the trailing edge ($\alpha_{45}S_DP_T$) when compared to the mid-span ($\alpha_{45}S_DP_O$) value. This suggests that the flow close to the leading edge is accelerated compared to the mid-span, while the flow close to the trailing edge is retarded. Similar observations over inclined ribs were reported by Bonhoff et al. (1999), Gao and Sunden (2004), and Tachie and Shah (2008). Bonhoff et al. (1999) argued that this complex variation of velocity is due to secondary motion that developed over inclined ribs. It was also reported that vortex created by the inclined ribs is driven towards the trailing edge of the ribs, and subsequently returns towards the leading edge of the ribs. The boundary layer parameters (δ, θ and H) also varied significantly with spanwise location. For example, in the parallel section, θ for $\alpha_{45}S_PP_L$ and $\alpha_{45}S_PP_T$ are both 45% lower than the value for $\alpha_{45}S_PP_O$. Meanwhile, in the diverging section, θ for $\alpha_{45}S_DP_T$ is 28% higher than obtained for $\alpha_{45}S_DP_O$, whereas the value for $\alpha_{45}S_DP_L$ is 28% lower.

Figure 4a demonstrates that in the parallel section there is a modest increase in U/U_m for $\alpha_{45}S_PP_L$, and a decrease in U/U_m for $\alpha_{45}S_PP_T$ compared with U/U_m for $\alpha_{45}S_PP_O$. However, in the diverging sections, the variation in U/U_m profiles in the spanwise direction is insignificant. Meanwhile, Tachie and Shah (2008) observed significant spanwise variation in their U/U_m profiles. The mean velocity profiles plotted in semi-log format are shown in Figure 4b, and Table 2 provides a summary of the drag characteristics. In the parallel section, C_f for $\alpha_{45}S_PP_L$ and $\alpha_{45}S_PP_T$ are, respectively, 31% and 72% higher than the value for $\alpha_{45}S_PP_O$. In the diverging section, C_f for $\alpha_{45}S_DP_L$ and $\alpha_{45}S_DP_T$ are, respectively, 19% and 8% higher than the value obtained for $\alpha_{45}S_DP_O$. The k_s^+ values obtained closed to the leading and trailing edges of the ribs in diverging sections are marginally higher than the minimum value of $k_s^+ = 70$ suggested for a fully rough regime (Schlichting, 1979).

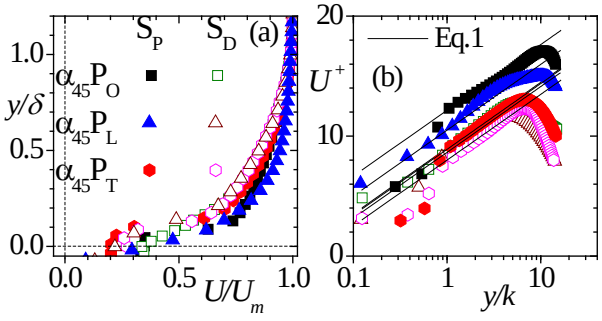

Figure 4. Mean velocity profiles at different spanwise locations: (a) outer coordinates (b) inner coordinates.

Figure 5 demonstrates that the Reynolds stresses close to the trailing edge are higher than those at the mid-span, whereas the distributions close to the leading edge are the least. Such an increase in the stresses close to the trailing edge is due to large scale events, such as violent eruption of fluid, which leads to a much stronger momentum transport. The Townsend structure parameter (Figure 5d) also varied along the spanwise direction. The maximum value of a_1 occurred near the leading edge and it is about 0.14 and 0.12, respectively, for $\alpha_{45}S_PP_L$ and $\alpha_{45}S_DP_L$. The a_1 for $\alpha_{45}S_PP_L$ however, decays more rapidly due to a slower decay of u^{+2} and v^{+2} compared to $-u^+v^+$.

Turbulence Structures

The quadrant decomposition and two-point velocity correlations are used to provide an insight into how APG and rib inclination angle modify the coherent structures. In quadrant decomposition, the ejection (Q2) and sweep (Q4) events are the most important events that contribute significantly to $-uv$. The inward (Q3) and outward (Q1) interaction motions do not contribute to $-uv$. The percentage contributions to $-uv$ from the various quadrant at the channel mid-span in both the parallel and diverging sections over the 90° and 45° ribs are shown in Figure 6. The present results over the 90° ribs in parallel section are in good agreement with results by Krogstad et al. (2005). The percentage

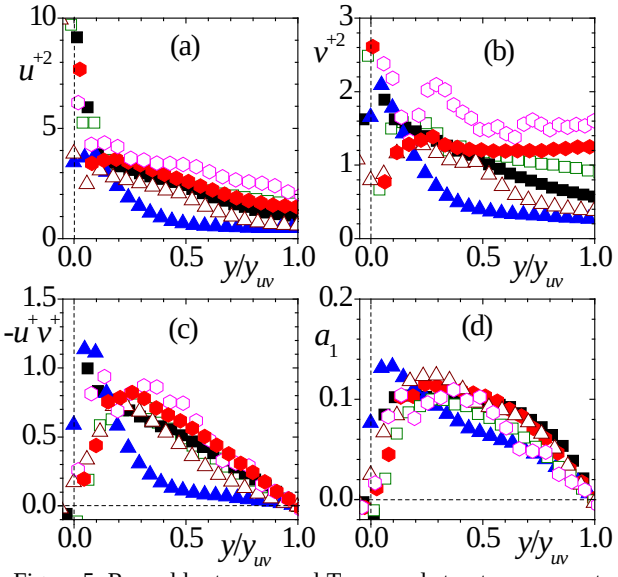

Figure 5. Reynolds stresses and Townsend structure parameter at different spanwise locations. Symbols as in Figure 4.

contribution from Q1 (Figure 6a) and Q3 (Figure 6c) to $-uv$ is always negative, and it increased in the presence of APG. Furthermore, these events are more intense over the 45° ribs than over the 90° ribs. Except for the Q2 events over the 90 ribs, these events are generally enhanced in the presence of APG. Moreover, the contributions from Q2 and Q4 over 45° the ribs are enhanced compared to that over 90° ribs. The rapid increase in Q2 away from the wall is likely due to the transport of low-momentum fluid from the wall towards the outer region. The near-wall spikes in Q4 may result from dominant turbulence transport towards the wall (Figure 6d). The Q4 event is stronger near the ribs, but decayed rapidly before increasing in the outer layer. The stronger Q4 events near the ribs are in agreement with the conjecture by Rapauch (1981) that Q4 accounts for most of the stresses close to the rough wall.

Over the 45° ribs the percentage contributions to $-uv$ from the various quadrants varied with spanwise location (Figure 7). In the parallel section, the contributions from Q1 and Q3 are least in the near-wall region of $\alpha_{45}S_PP_L$, but these motions increased rapidly away from the rough wall. For $y/y_{uv} > 0.54$, Q1 and Q3 motions for $\alpha_{45}S_PP_T$ are relatively stronger than those at mid-span but weaker than those for $\alpha_{45}S_PP_L$. The Q2 and Q4 events beyond $y/y_{uv} = 0.16$ and $y/y_{uv} = 0.40$ for $\alpha_{45}S_PP_L$ are more intense than observed for $\alpha_{45}S_PP_O$ and $\alpha_{45}S_PP_T$. In the diverging section, Q1 and Q3 events for $\alpha_{45}S_DP_L$ are weaker than those for $\alpha_{45}S_DP_O$ and $\alpha_{45}S_DP_T$. Moreover, Q2 events for $\alpha_{45}S_DP_T$ dominate for $y/y_{uv} \leq 0.12$, but beyond this location the Q2 events for $\alpha_{45}S_DP_O$ were strengthened. The Q4 events at the mid-span are relatively stronger than those obtained at the other spanwise locations in the diverging section.

Figure 8 shows contours of two-point correlations of the streamwise fluctuating velocity, R_{uu} centred at $y_{ref}/\delta = 0.4$. The

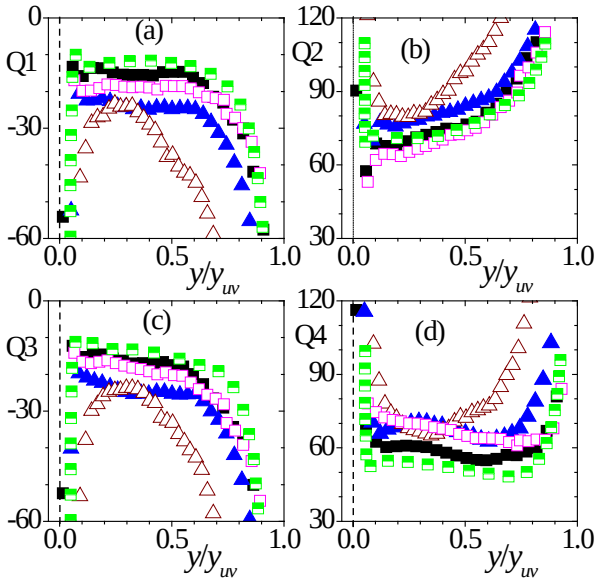

Figure 6. Percentage contribution by the quadrants at the mid-span of the channel. Symbols as in Figure 2, and Krogstad et al. (2005): ▭.

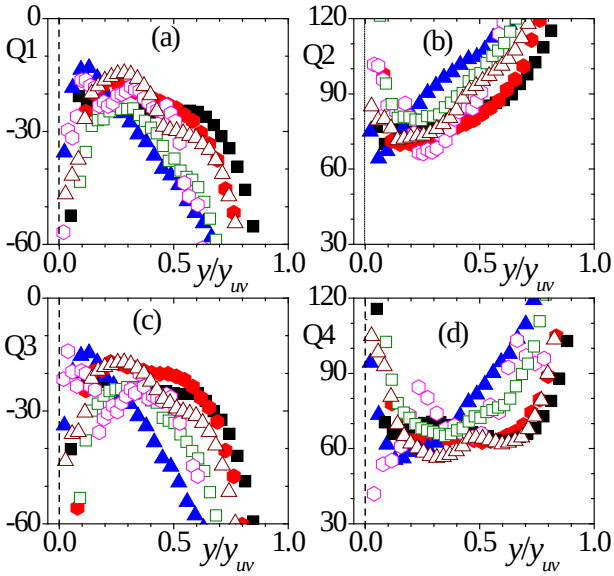

Figure 7. Percentage contribution by the quadrants at different spanwise locations. Symbols as in Figure 4.

plots are used to quantify the average extent, inclination angle and shape of hairpin packets. The R_{uu} contours at various locations over the ribs are elliptical in shape and they are elongated in the streamwise direction. The streamwise length scale Lx_{uu} of R_{uu} was estimated as twice the distance from self-correlation peak to the most downstream location on the R_{uu} = 0.5 contour (Christensen and Wu, 2005). The wall-normal length scale Ly_{uu} of R_{uu} also corresponds to wall-normal distance between the points closest and farthest from the wall on a particular contour level. These length scales as well as the inclination angle for the hairpin packets, β are summarised in Table 3. Over the 90° ribs, the difference between Lx_{uu} in the parallel and diverging sections is insignificant, but an increase is observed in the diverging section for the 45° ribs at mid-span. Meanwhile, Ly_{uu} increased with APG. Generally, Lx_{uu} and Ly_{uu} are larger over the 90° ribs than over the 45° ribs. In the parallel section, Lx_{uu} and Ly_{uu} for $\alpha_{45}S_PP_L$ are higher than those for $\alpha_{45}S_PP_O$, but lower than those for $\alpha_{45}S_PP_T$. However, in the diverging section, Lx_{uu} is independent of spanwise measurement location. The difference between Ly_{uu} for $\alpha_{45}S_DP_O$ and $\alpha_{45}S_DP_L$ is 11.4% and that for $\alpha_{45}S_DP_O$ and $\alpha_{45}S_DP_T$ is only 6%. Also the inclination angle, β of the hairpin

Table 3. Average size and inclination angle of hairpin packets.

Test	β (°)	Lx_{uu}/δ	Ly_{uu}/δ
$\alpha_{90}S_PP_O$	7.4	0.93	0.34
$\alpha_{90}S_DP_O$	13.0	0.90	0.39
$\alpha_{45}S_PP_O$	−3.5	0.40	0.23
$\alpha_{45}S_DP_O$	9.0	0.67	0.35
$\alpha_{45}S_PP_L$	−4.5	0.35	0.18
$\alpha_{45}S_DP_L$	8.1	0.67	0.31
$\alpha_{45}S_PP_T$	5.5	0.85	0.35
$\alpha_{45}S_DP_T$	−2.7	0.67	0.33

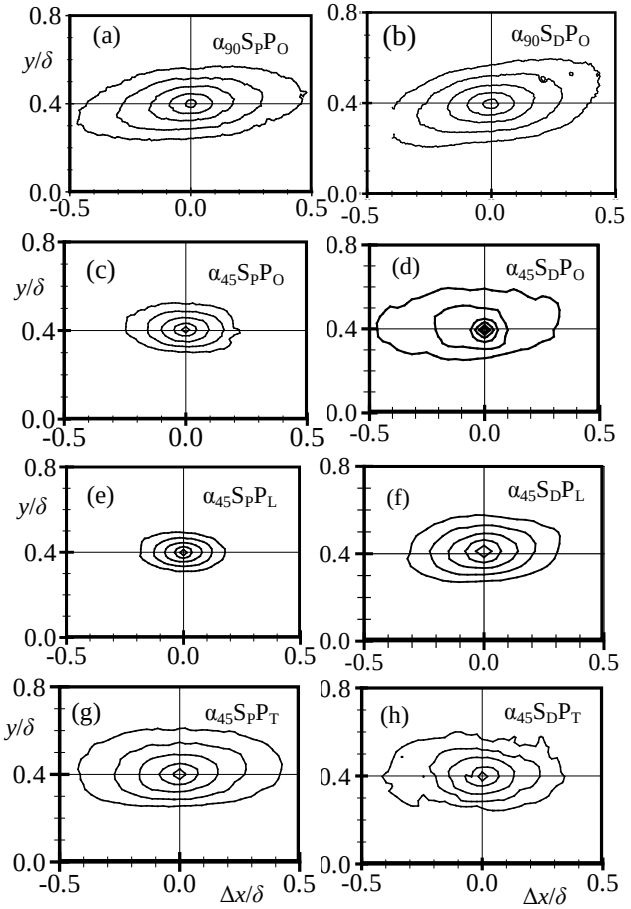

Figure 8. Contours of R_{uu} centred at y/δ = 0.4, outermost contour R_{uu} = 0.5, and contour spacing at 0.1.

packets increases with APG, and it is larger for the 90° ribs than 45° ribs. The negative β over 45° ribs indicates that R_{uu} is tilted towards the ribs. Tachie et al. (2009) also reported negative values for β.

SUMMARY AND CONCLUSIONS

The present results revealed that 45° ribs reduced the drag characteristics compared to perpendicular ribs. It was also observed that APG enhanced turbulence level, especially for 90° ribs. For the present test conditions, APG reduced the drag over 90° rib but increased the drag over the 45° rib. Quadrant analysis and two-point velocity correlations showed imprints of hairpin packets in the flow. It was found that sweep events are dominant contributors to the Reynolds shear stress in the near-wall region, but away from the ribs ejection contributes significantly to $-uv$. The R_{uu} demonstrates that there is a long streamwise correlation of low-speed fluid regions over the perpendicular ribs compared to the 45° rib. Similarly, the wall-normal length scale estimated from R_{uu} is larger for the 90° rib than for the 45° rib. Considerable variation of the quadrant events and size associated with the hairpin packets were also observed in the spanwise directions over the 45° rib.

REFERENCES

Bonhoff, S. B., Parneix, S., Leusch, J., Johnson, B. V., Schabacker, J., and Bölcs, A., 1999, "Experimental and numerical study of developed flow and heat transfer in coolant channels with 45 degree ribs", *Int. Journal of Heat and Fluid Flow*, Vol. 20, pp. 311–319.

Bradshaw, P., 1967, "The turbulent structure of equilibrium turbulent boundary layers", *Journal of Fluid Mech.*, Vol. 29, pp. 625-645.

Christensen, K. T., and Wu, Y., 2005, "Characteristics of Vortex Organisation in the Outer Layer of Wall Turbulence", *Proceedings, 4th International Symposium on Turbulence and Shear Flow Phenomena*, Williamsburg, Virginia, Vol. 3, pp. 1025-1030.

Gao, X., and Sunden, B., 2004, "Effects of Inclination Angle of Ribs on the Flow Behaviour in the Rectangular Ducts ", *Journal of Fluid Eng.*, Vol. 126, pp. 692-699.

Han, J. C., Glicksman, L. R, and Rohsenow, W. M., 1978, "An Investigation of Heat Transfer and Friction for Rib-Roughened Surfaces", *Intl. Journal of Heat and Mass Transfer*, Vol. 21, pp.1143-1156.

Hanjalic, K., and Launder, B. E., 1972, "Fully developed asymmetric flow in a plane channel", *Journal of Fluid Mech.*, Vol. 51, pp. 301-335.

Ikeda, T., and Durbin, P., 2007, "Direct simulations of a rough-wall channel flow", *Journal of Fluid Mech.*, Vol. 571, pp. 235-263.

Krogstad, P.-Å., Andersson, H. I., Bakken, O. M., and Ashrafian, A., 2005, "An Experimental and Numerical Study of Channel Flow with Rough Walls", *Journal of Fluid Mech.*, Vol. 530, pp. 327-352.

Nagano, Y., and Tagawa, M., 1995, "Coherent Motions and Heat Transfer in a Wall Turbulent Shear Flow", *Journal of Fluid Mech.*, Vol. 305, pp. 127-157.

Perry, A.E., Schofield, W. H., and Joubert, P. N., 1969, "Rough Wall Turbulent Boundary Layers", *Journal of Fluid Mech.*, Vol. 37, pp. 383-413.

Rapauch, M. R., 1981,"Conditional Statistics of Reynolds Stress In Rough-Wall and Smooth-Wall Turbulent Boundary Layers", *Journal of Fluid Mech.*, Vol. 108, pp. 363-382.

Schlichting, H., 1979, *Boundary-Layer Theory"* (McGraw-Hill, New York)

Schwarz, W. R., and Bradshaw, P., 1994, "Turbulence Structural Changes for a Three-Dimensional Turbulent Boundary Layer in a 30° Bend", *Journal of Fluid Mech.*, Vol. 272, pp. 183-210.

Tachie, M. F., 2007, "Particle Image Velocimetry Study of Turbulent Flow over Transverse Square Ribs in an Asymmetric Diffuser", *Physics of Fluids*, Vol. 19, pp. 1-15.

Tachie, M. F., and Shah, M. K., 2008, "Favourable Pressure Gradient Flow over Straight and Inclined Ribs on Both Channel Walls ", *Physics of Fluids*, Vol. 20, pp. 1-22.

Tachie, M. F., Paul, S. S., Agelinchaab, M., and Shah, M. K., 2009, "Structure of Turbulent Flow Over 90° and 45° Transverse Ribs", *Journal of Turbulence*, Vol. 10, pp. 1-20.

Tay, G. F. K., Kuhn, D. C. S., and Tachie, M. F., 2009, "Influence of adverse pressure gradient on rough-wall turbulent flows", *Int. Journal of Heat and Fluid Flow*, Vol. 30, pp. 249-265.